SANDIA REPORT

SAND2003-2422
Unlimited Release
Printed August 2003

Mechanical Behavior, Properties and Reliability of Tin-Modified Lead Zirconate Titanate

Chad S. Watson

Prepared by
Sandia National Laboratories
Albuquerque, New Mexico 87185 and Livermore, California 94550

Sandia is a multiprogram laboratory operated by Sandia Corporation,
a Lockheed Martin Company, for the United States Department of Energy under Contract DE-AC04-94AL85000.

Issued by Sandia National Laboratories, operated for the United States Department of Energy by Sandia Corporation.

Available to DOE and DOE contractors from
U.S. Department of Energy
Office of Scientific and Technical Information
P.O. Box 62
Oak Ridge, TN 37831

Telephone: (865)576-8401
Facsimile: (865)576-5728
E-Mail: reports@adonis.osti.gov
Online ordering: http://www.doe.gov/bridge

Available to the public from
U.S. Department of Commerce
National Technical Information Service
5285 Port Royal Rd
Springfield, VA 22161

Telephone: (800)553-6847
Facsimile: (703)605-6900
E-Mail: orders@ntis.fedworld.gov
Online order: http://www.ntis.gov/ordering.htm

SAND2003-2422
Unlimited Release
Printed August 2003

Mechanical Behavior, Properties and Reliability of Tin-Modified Lead Zirconate Titanate

Chad S. Watson
Ceramic Materials Department
Sandia National Laboratories
PO Box 5800, MS 0889
Albuquerque, New Mexico 87185

ABSTRACT

The influences of temperature and processing conditions (unpoled or poled-depoled) on strength, fracture toughness and the stress-strain behavior of tin-modified lead zirconate titanate (PSZT) were evaluated in four-point bending. PSZT exhibits temperature-dependent non-linear and non-symmetric stress-strain behavior. A consequence of temperature dependent non-linearity is an apparent reduction in the flexural strength of PSZT as temperature increases. At room temperature the average stress in the outer-fiber of bend bars was 84 MPa, whereas, for specimens tested at 120°C the average failure stress was only 64 MPa. The load-carrying capacity, however, does not change with temperature, but the degree of deformation tolerated by PSZT prior to failure increased with temperature.

ACKNOWLEDGEMENTS

Technical contributions by Michael Hutchinson, George Burns, Bonnie Mckenzie, John Laing, Roger Moore, Pin Yang and Jill Glass are gratefully acknowledged. Sandia is a multiprogram laboratory operated by Sandia Corporation, a Lockheed Martin Company, for the United States Department of Energy's National Nuclear Security Administration under Contract DE-ACO4-94-AL85000.

CONTENTS

FIGURES

TABLE

INTRODUCTION

Partially electroded ferroelectric devices that are heated to enhance dipole alignment under the influence of an electric field develop differential strains at the electrode edge. Strain incompatibilities at the electrode boundary can result in stresses large enough to initiate cracks from nearby flaws[1-3]. Similarly, multilayer actuators, which are composed of several layers of partial internal electrodes, can develop stresses during switching operations that are high enough to generate cracks at electrode boundaries, thus limiting the effective lifetime of the device[4]. The reliability of partially electroded ferroelectrics can be improved by using thinner layers, which effectively reduces the volume of material exposed to high tensile stresses around the electrode edge during poling[2, 3]. Another reliability enhancement technique includes the use of a pre-conditioning step prior to polarizing the electroded volume. By polarizing and then depolarizing the entire ferroelectric element, the domains in the material, instead of being randomly oriented, are now aligned "parallel" to the applied field. As a result, the strain differential between the electroded and unelectroded area can be reduced; for example, from ~800 $\mu\varepsilon$ to only 200 $\mu\varepsilon$ in the ε_{31} direction for tin-modified lead zirconate titanate[1].

Frequently, ferroelectric devices are exposed to elevated temperatures, during processing or while in operation, which could potentially degrade component integrity. For instance, the mechanical properties of ferroelectrics can vary as temperature is increased due to phase transformations, domain wall movement, residual stress changes, microcracking or other mechanisms. Research relating the effect of temperature on the mechanical properties of ferroelectrics indicates a reduction in strength[5, 6] and fracture toughness[7] as the applied temperature approaches the Curie point. The potential for temperature-dependent mechanical degradation of ferroelectrics needs to be addressed to establish a more complete understanding of component reliability. To this end, the effect of temperature on the stress-strain behavior, flexural strength and fracture toughness of tin-modified lead zirconate titanate (PSZT) have been examined. In addition, Weibull strength parameters were determined for unpoled and poled-depoled specimens at room temperature.

EXPERIMENTAL PROCEDURE

Conventional mixed oxide techniques were used to prepare sintered PSZT (Alliant Corporation, New Hope, MN). Bend bars were sliced and ground from sintered billets (HF6104) and finished with a 600 grit diamond wheel to dimensions of 3 mm x 4 mm x 45 mm. Analogous to the procedures used to fabricate PSZT partially electroded components, all of the bend bars were thermally cleaned at 825°C. At this point, the bend bars were in the unpoled state, i.e., the domains in the material were assumed to be randomly oriented. Some of these unpoled bend bars were saved after thermal cleaning for mechanical property measurements. The remaining bend bars were processed through the pole-depole state. A temporary silver electrode was applied to the top and bottom surface of the bend bars and dried at 71°C. After the temporary electrode was dried and the bend bar cooled to room temperature, it undergoes a pole-depole process.

For this process, the bend bars were polarized in dielectric fluid (Fluorinert FC77, 3M Corp., Minneapolis, MN) at room temperature to 32 kV/cm; whereupon, the electric field was reversed until negligible charge was stored. After pole-depole the temporary electrode was removed by rinsing in acetone. A schematic illustrating the polarization and depolarization sequence is shown in Fig. 1 and the experimental configuration of the bend bars with respect to the poling-depoling direction and loading conditions is shown in Fig. 2.

Flexure strength, fracture toughness and stress-strain behavior of PSZT were measured in four-point bending at 23, 75, 86, 100 and 120°C. For the 75, 86 and 100°C runs, the samples were taken to 105°C and held at temperature for 15 min and then cooled to their respective test temperature at 3°C/min and held at temperature for 15 min prior to testing to minimize thermal gradients in the material. These heating and cooling cycles (3°C/min ramp rates and 15 min holds) are analogous to those used for hot poling PSZT components. A MTS 810 Universal Testing Machine and a MTS Environmental

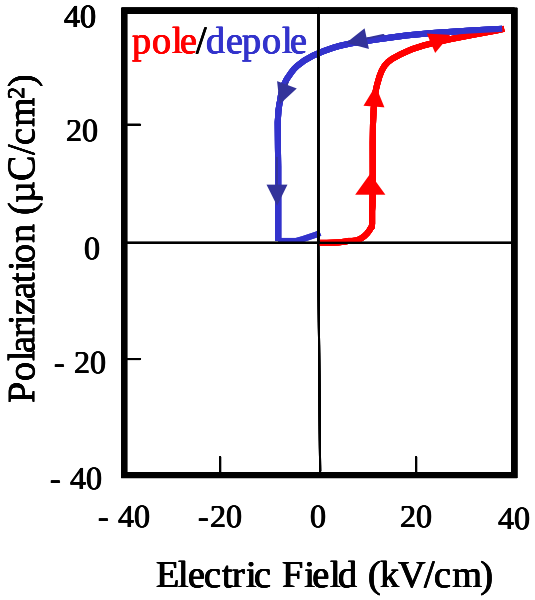

Fig. 1 Schematic of the polarization and depolarization (pole-depole) sequence.

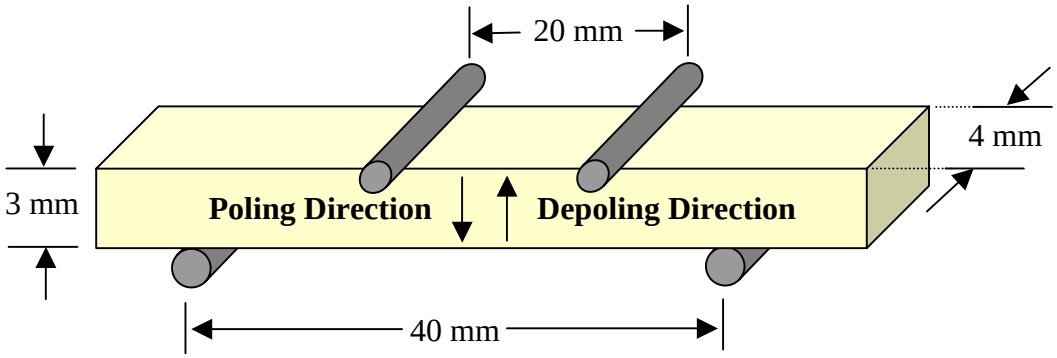

Fig. 2 Schematic of bend bar geometry and polarization direction.

Chamber (MTS Systems Corporation, Minneapolis, MN) were used to mechanically load the specimens at temperature.

Strength was measured according to ASTM C1161-02c[8] and fracture toughness was measured using the indentation-crack length[9] and indentation-strength[10] method. In addition, Weibull parameters for unpoled and poled-depoled PSZT were determined from room temperature strength measurements. For indentation-crack length measurements, a 49 N Vickers indentor was loaded onto an optically polished specimen for 15 sec. Indentation-strength measurements were made by loading a Vickers indentor on the 4 mm wide tensile face of bend bars for 15 sec. Care was taken to ensure that two of the radial cracks emanating from opposite corners of the indentation were aligned perpendicular to the long axis of the bend bar. Silicone oil was placed over the indentation to inhibit slow crack growth and samples were loaded to failure at 0.5 mm/min or 12.3 MPa/s.

To evaluate the stress-strain behavior of PSZT, load-strain and load-deflection measurements were performed at each temperature condition. Tensile and compressive strains that developed while loading to failure were determined for two specimens at each temperature with the use of strain gauges with pre-attached leads (Type CEA-06-062UW-350, Measurements Group, Inc.; Raleigh, NC). The gauges were affixed to the compression and tension face of the bend bars with adhesive (M-Bond 600; Measurements Group, Inc.; Raleigh, NC) and cured at 100°C for four hours. Deflection measurements were made on eight specimens at each temperature utilizing an extensometer (MTS Systems Corporation, Minneapolis, MN). The deflection data was converted to strain (ε),

$$\varepsilon = \frac{6Wh}{L^2} \tag{1}$$

where W is the magnitude of bar deflection, h is bar thickness and L is the distance between the outer supports.

Representative SEM micrographs of a polished and chemically etched PSZT specimen and of a typical fracture surface are shown in Figs. 3a & b, respectively. PSZT

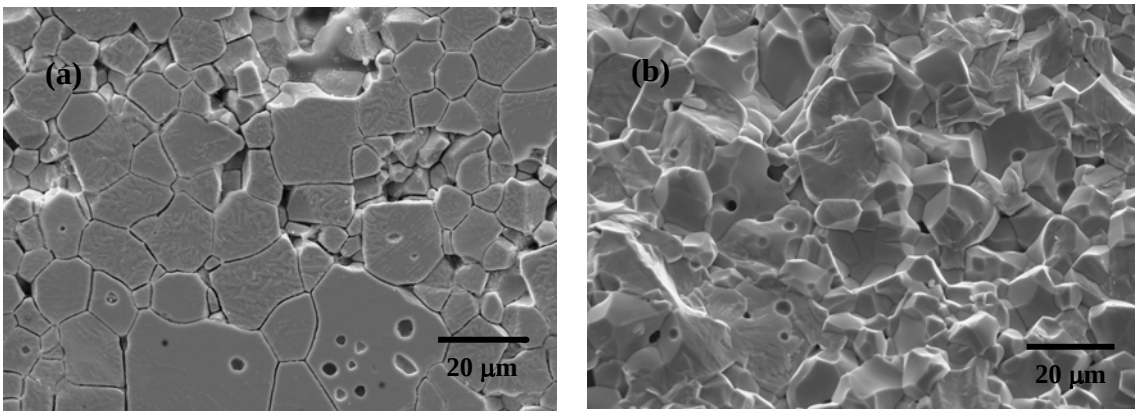

Fig. 3 SEM images of (a) polished and chemically etched PSZT and (b) of a typical fracture surface.

microstructures consist of equiaxed grains with a bimodal grain size distribution. Some intragranular porosity within the larger grains is evident. The grain pullout is an artifact of polishing. PSZT fractures in both an intergranular and transgranular mode. Typically, the larger grains fail transgranularly while smaller grains fail intergranularly.

RESULTS AND DISCUSSION

Non-Linear Stress-Strain Behavior and True Flexural Strength

From the load-strain and load-deflection measurements, it was found that PSZT exhibits non-linear stress-strain behavior. A plot of linear-elastically computed stress (or engineering stress) versus strain for poled-depoled specimens tested at room temperature, 75, 86, 105 and 120°C is shown in Fig. 4. Deviations from linear-elastic behavior initiate at a nominal stress level of approximately 20-30 MPa for specimens tested at room temperature and 10-20 MPa for specimens tested at an elevated temperature. Furthermore, the extent of non-linearity increases as the testing temperature increases. Conversion of the load-strain data to the true stress-strain behavior was achieved by implementing the approach first described by Nadai[11] and adapted by Chen *et al*[12]. The true compressive (σ_c) and tensile stresses (σ_t) were calculated as follows:

$$\sigma_c = \frac{2M(\varepsilon_t - \varepsilon_c)}{\varepsilon_c bh^2} - \frac{\partial M}{\partial \rho}\frac{1}{\varepsilon_c bh} \tag{2}$$

$$\sigma_t = \frac{2M(\varepsilon_t - \varepsilon_c)}{\varepsilon_t bh^2} - \frac{\partial M}{\partial \rho}\frac{1}{\varepsilon_t bh} \tag{3}$$

where M is the applied bending moment, ε_c and ε_t are the compressive and tensile strains respectively, b is the width of the bend bar, and ρ is radius of curvature given by

$$\rho = \frac{h}{\varepsilon_t - \varepsilon_c} \tag{4}$$

The true stress versus strain curves are shown in Fig. 5. These curves are derived from the same load-strain data as the engineering stress-strain curves in Fig. 4. It is evident that as the temperature increases, the amount of deformation supported by the material to failure also increases. For example, the specimen tested at room temperature failed at a strain of ~800 με, whereas, the specimen tested at 120°C deformed twice as much at failure (~1600 με). This additional deformation is most likely the result of a higher percentage of domains switching in response to the applied load.

The reproducibility of the stress-strain measurements is shown in Fig. 6 where the true tensile stress-strain traces of two strain-gauged specimens at each temperature follow similar curves. Assuming the remaining eight bend bars that were tested to failure without a strain gauge at each temperature exhibit a similar stress-strain response, then

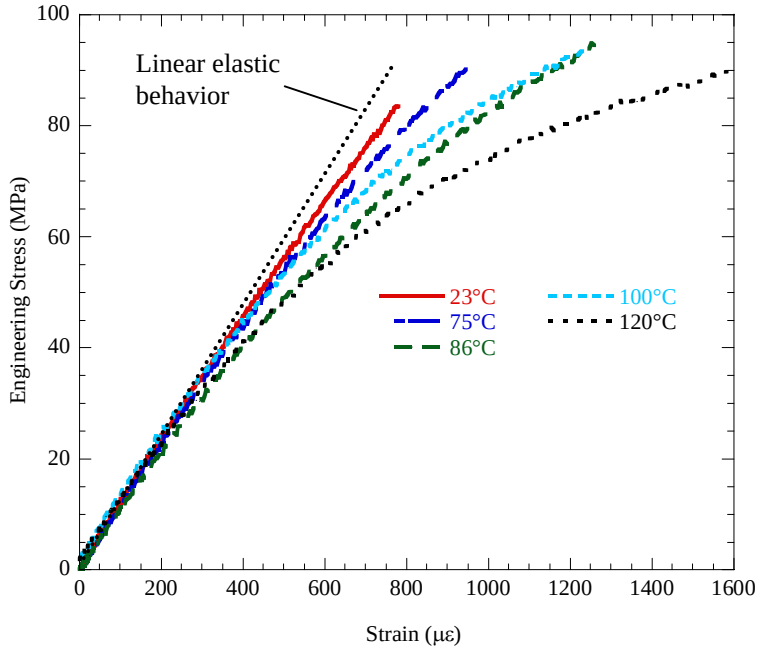

Fig. 4 Tensile stress-strain curves to failure for PSZT four-point bend specimens at 23, 75, 86, 100 and 120°C assuming linear-elasticity.

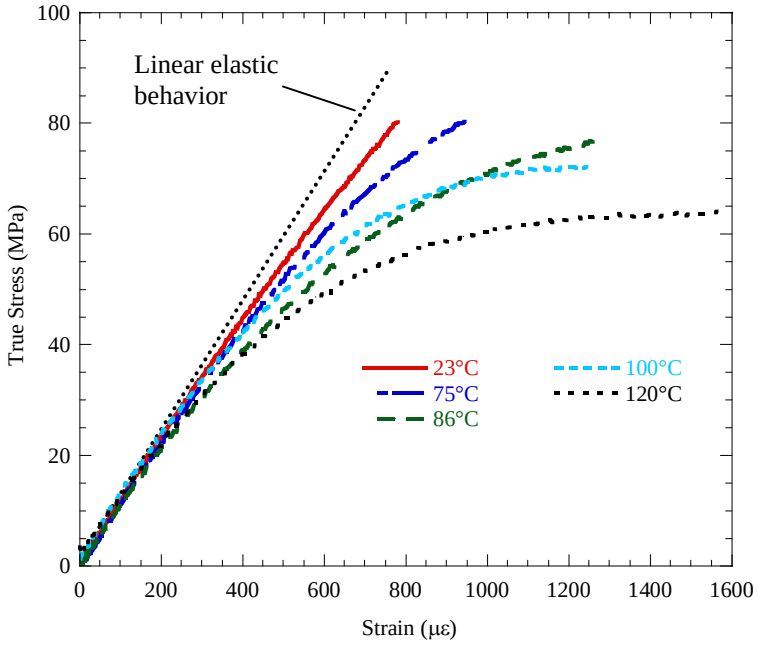

Fig. 5 Conversion of load-strain data to the true tensile stress-strain curves to failure for PSZT four-point bend specimens at 23, 75, 86, 100 and 120°C.

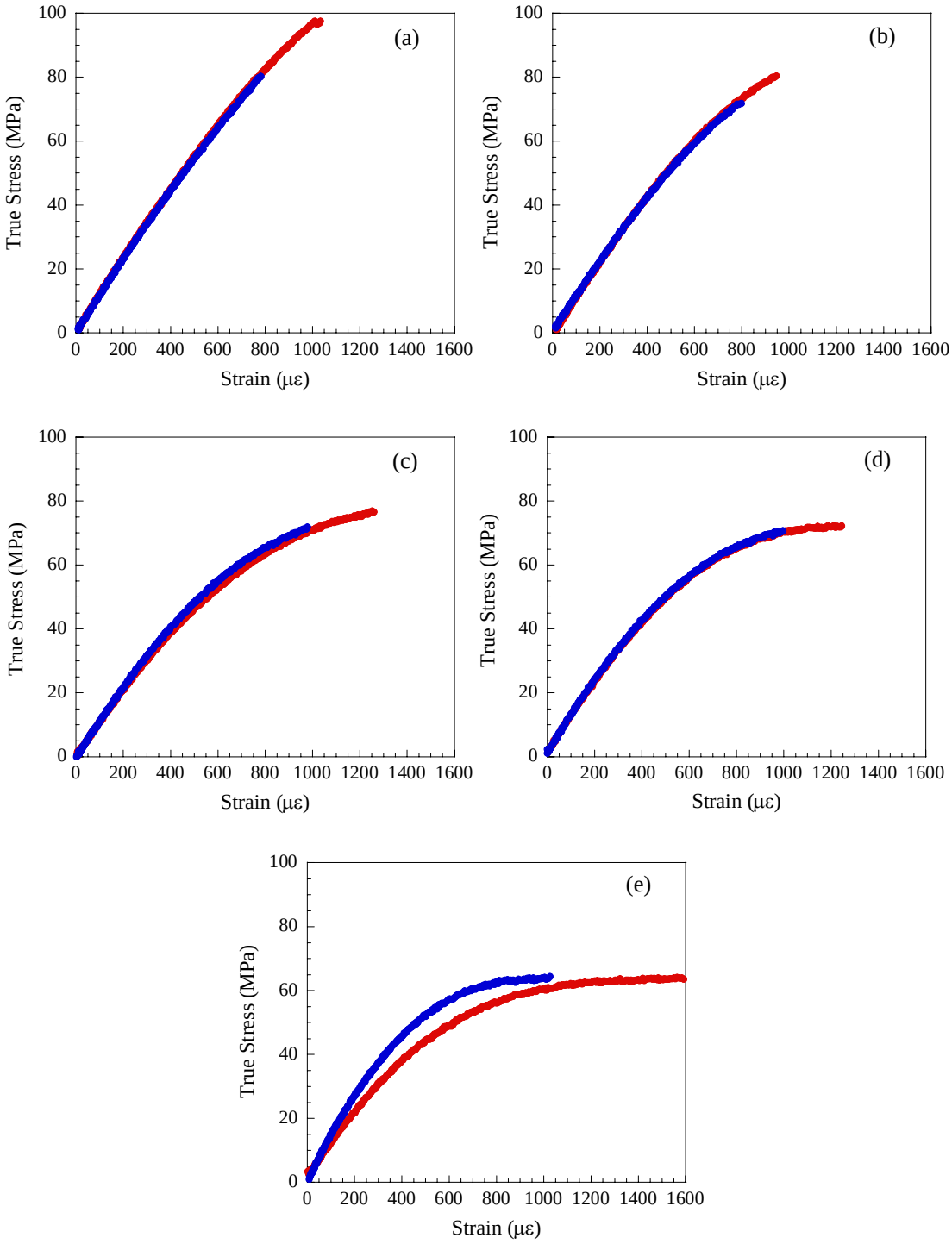

Fig. 6 True tensile stress-strain curves to failure of two different strain-gauged PSZT four-point bend specimens at (a) 23, (b) 75, (c) 86, (d) 100 and (e) 120°C.

the true failure stress for each specimen can be determined. High-order polynomial trendlines of true stress versus load for each strain-gauged specimen were generated. The load at failure was then placed into the polynomial equation solving for the true failure stress. The average true failure stress based on the stress-strain response of the two strain-gauged specimens, per temperature, is shown in Table I and Fig. 7. In addition, the average load at failure, linear elastic or engineering stress, true stress calculated from displacement data and fracture toughness as a function of temperature are given in Table I. The linear elastic or engineering stress and the true stress calculated from displacement data are also shown in Fig. 7.

At room temperature, soft PZT-based materials can exhibit non-linear and non-symmetric behavior[13]. Reports of the strength and fracture toughness of soft PZT-based materials or even other ferroelastic materials without direct knowledge of non-linearity and non-symmetry, in the case of flexure tests, can result in misleading data. To fully

TABLE I: Mechanical Property Measurements with 95% Confidence Intervals

Temperature	Failure Load (N)	Engineering Failure Stress (MPa)	True Failure Stress (MPa) – Strain Gauges	True Failure Stress (MPa) - Extensometer	Fracture Toughness ($MPa \cdot m^{1/2}$)
23°C*	103.9 ± 6.3	86.0 ± 5.3	83.9 ± 6.7	82.2 ± 4.6	1.81 ± 0.28
23°C	106.2 ± 8.3	88.0 ± 6.9	84.3 ± 6.1	82.3 ± 5.1	1.85 ± 0.16
75°C	110.9 ± 5.7	91.7 ± 4.5	82.1 ± 3.1	82.0 ± 3.5	1.74 ± 0.09
86°C	105.7 ± 5.6	87.7 ± 4.6	73.9 ± 2.3	76.8 ± 2.9	1.85 ± 0.06
100°C	108.0 ± 3.6	89.5 ± 2.8	71.6 ± 0.7	72.7 ± 1.8	1.71 ± 0.03
120°C	100.7 ± 4.3	83.8 ± 3.5	63.7 ± 0.7	65.4 ± 2.1	1.81 ± 0.28

*Unpoled Specimen

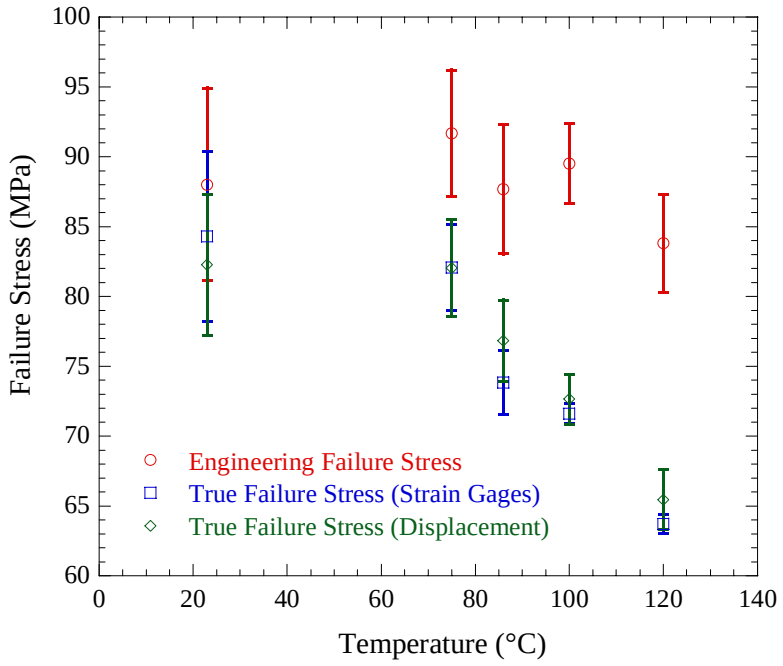

Fig. 7 Average engineering and true (strain gauge and displacement technique) failure stress with 95% confidence intervals from room temperature to 120°C.

complement strength data, it is recommended that when flexural strength measurements of ferroelectrics are reported that the stress-strain behavior of the material also be included. Otherwise, without full disclosure of stress-strain behavior, the predicted strength of the material, as that calculated from linear-elastic fracture mechanics can lead to a systematic over-estimation of strength (Fig. 7). Indeed, the most appropriate method for reporting strength data without strain-gauge or deflection measurements is load at failure (Table I). With this disclosure, at least the load-carrying capacity of the material is identified.

Because strain-gauge measurements can be cumbersome, strain development can also be assessed from deflection measurements using an extensometer. However, extensometers do not provide the same sensitivity as strain-gauges. In addition, contributions from non-symmetry are not measured with an extensometer. Nonetheless, the true strength can be ascertained, but non-symmetry contributions are assumed negligible and strain resolution is compromised. The true failure stress of specimens loaded to failure without strain-gauges was determined where the load-deflection measurements made with an extensometer were converted to the true failure stress following Gogotsi[14],

$$\sigma_t = \frac{3a}{bh^2}\left(P + \frac{\varepsilon}{2}\cdot\frac{dP}{d\varepsilon}\right) \tag{5}$$

where a is the distance between the inner supports, P is the load, and ε is the tensile strain (calculated using Eq. 1) experienced by the material during flexure. A small portion of the load-deflection data (three out of eight poled-depoled specimens at 23°C and one out of eight poled-depoled specimens at 120°C) was taken from measurements made with the LVDT of the mechanical testing machine. In addition, the strains measured with the two strain-gauge experiments at each temperature were also included in the extensometer data set, as a result, a total of ten specimens were averaged to determine the true failure stress using Eq. 5. The results are given in Table I and shown in Fig. 7. The true failure stresses, as calculated from the strain-gauge and displacement techniques are typically within 3%. As shown in Fig. 7, the average true stresses for both measurement techniques follow the same trend: the true failure stress decreases with increasing temperature. At room temperature, the true failure stress as calculated using the strain gauge technique is 84.3 MPa and decreases significantly to 63.7 MPa by 120°C. However, if we were to assume that the material behaved linearly elastically, the true failure stress would have been overestimated by ~4% at room temperature and ~24% at 120°C. The increase in the difference between the engineering stress and the true failure stress as temperature increases is because non-linearity increases with temperature. Although the true failure stress decreases with temperature, the load-carrying capacity of PSZT does not differ significantly with 95% confidence. The average load at failure is between 100.7 and 110.9 N over the entire temperature range. Thus, the material is able to support similar loads prior to failure while also being able to support a higher degree of deformation as temperature increases. Intuitively, this suggests that at elevated temperatures PSZT is able to alleviate mechanically induced stresses by deforming.

Stress-Strain Behavior of Unpoled and Poled-Depoled PSZT

A distinct difference in the stress-strain response of unpoled and poled-depoled PSZT, as measured with strain gauges, is shown in Fig. 8. Poled-depoled PSZT exhibits additional non-linearity. This trend would most likely continue until the Curie temperature is reached. Presumably, the difference in the non-linearity is the result of the formation of 180° domains parallel to the applied electric field (or as close as crystallographically possible) during the polarization and depolarization step. Because domains attempt to align parallel to the direction of maximum principal stresses in tension, which is perpendicular to the polarization-depolarization direction, a higher percentage of domains in the poled-depoled specimen are available for switching. For the unpoled specimen, domains are randomly oriented, thus certain percentages are already parallel or nearly parallel to the direction of maximum principal stresses; therefore, fewer domains are available for switching during loading.

Non-Symmetrical Stress-Strain Behavior

PSZT, as with similar soft ferroelastics, exhibits non-symmetric stress-strain behavior[13]. Non-symmetry was negligible at room temperature for PSZT but at elevated temperatures non-symmetry was evident (Fig. 9a-e). However, because of strain-gauge misalignment, poor strain-gauge adhesion, or statistical variations in data, not all of the elevated temperature stress-strain tests revealed significant non-symmetrical behavior (Appendix). Non-symmetry refers to deviations in the stress-strain response in tension as compared to compression. In response to tension, domains align parallel to the principal stress direction, and in compression domains align perpendicular to the principal stress

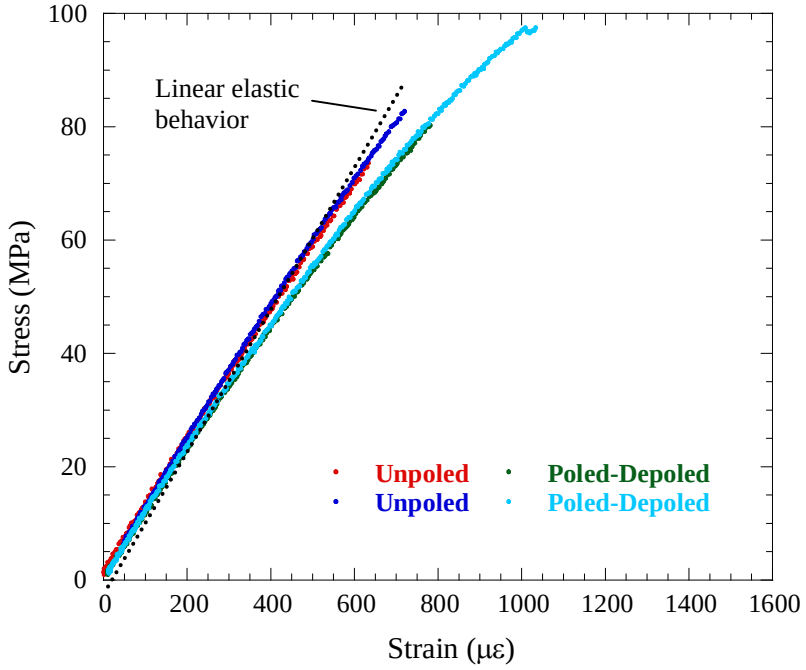

Fig. 8 True tensile stress-strain behavior (strain gauge technique) of unpoled and poled-depoled PSZT at room temperature.

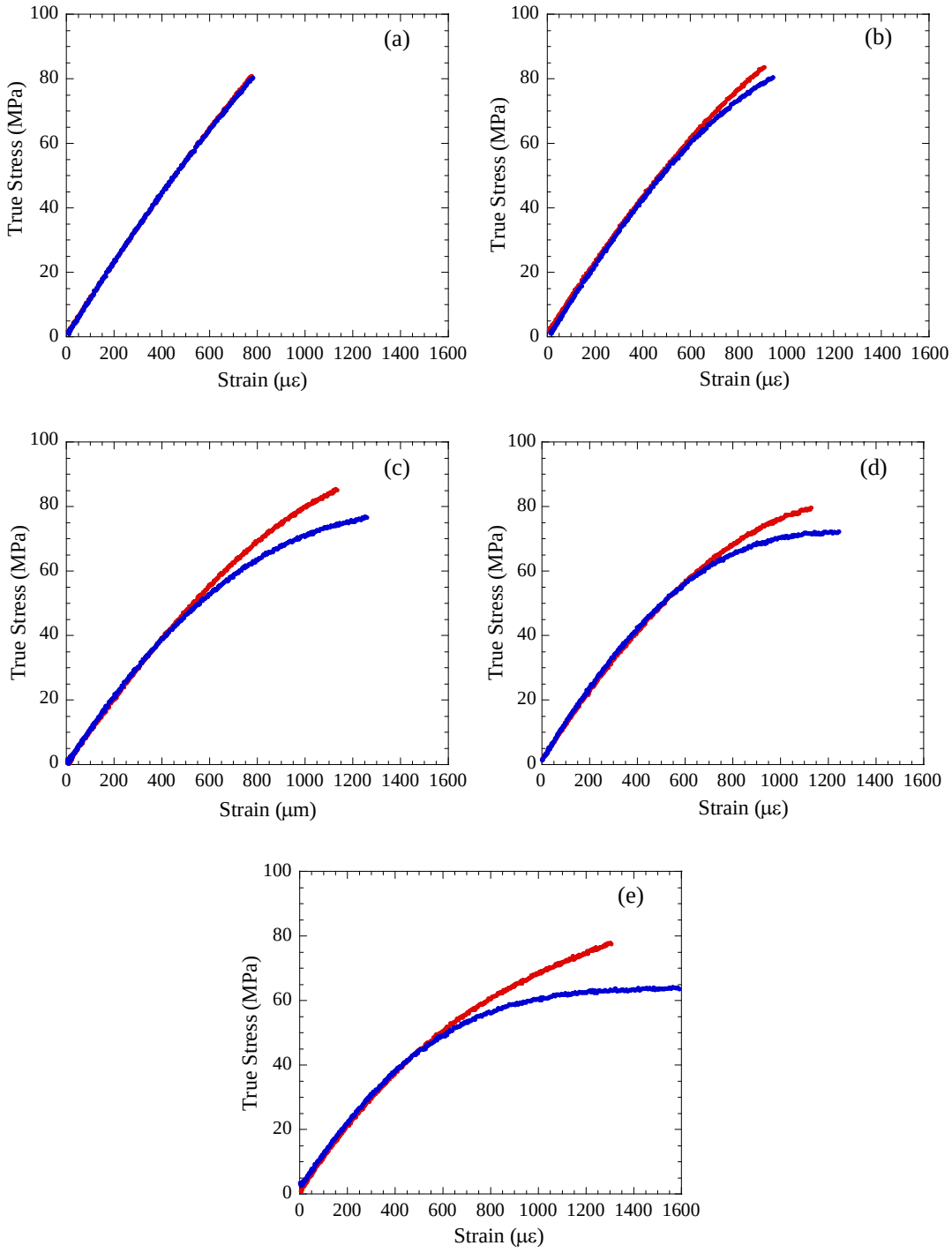

Fig. 9 Non-symmetry is evident by comparing the tension (blue curve) and the compressive (red curve) stress-strain curves to failure for PSZT four-point bend specimens at (a) 23, (b) 75, (c) 86, (d) 100 and (e) 120°C

direction. As a result, at the same loading level, above which non-linearity has developed, the resulting strain in a specimen poled perpendicularly to the maximum principal direction (or for an unpoled specimen) is greater in tension than in compression. As a consequence the outer-fiber stress of a perpendicularly poled or unpoled specimen tested in flexure is greater in compression than in tension. Comparisons of non-symmetry obtained through flexure testing to measurements made from simple uniaxial compression and tension tests follow the same trends. But by applying strain gauges on the compression and tension faces of bend bars, non-symmetry can easily be ascertained[13]. In doing so, the intrinsic variability of material properties can be avoided because both the compression and tension response can be determined for the same test specimen instead of two independent test specimens needed for compression and tension tests.

Fracture Toughness

Fracture toughness values were calculated using both the indentation-crack length[9] and indentation-strength[10] techniques. For the indentation-crack length technique, fracture toughness measurements were made at room temperature on unpoled specimens. By indenting a specimen with a Vickers indentor and measuring the average length of the radial cracks (2c) emanating from the hardness impression, the fracture toughness can be obtained with the following equation:

$$K_{Ic} = 0.016\left(\frac{E}{H}\right)^{\frac{1}{2}} \bullet \left(\frac{P}{c^{\frac{3}{2}}}\right) \tag{6}$$

where E is the modulus and P is the indentation load. Hardness (H) was determined for each indent by measuring the average length of the two diagonals (d):

$$H = \frac{2P}{d^2} \tag{7}$$

A total of eight hardness impressions was used to determine the average indentation-crack length toughness. With an indentation load of 49 N and an elastic modulus of 130.4 GPa[15], an average indentation-crack length toughness of 2.12 ± 0.11 MPa·m$^{1/2}$ was obtained.

The fracture toughness of PSZT was measured at 23, 75, 86, 100 and 120°C using the indentation-strength technique. Vickers indents were applied to the tensile surface of bend bars with a 49 N load, which developed cracks on the order of 380 μm in length. The bend bars were then loaded in flexure until the indentation flaw initiated final failure. The average indentation-strength fracture toughness was calculated with the following relationship:

$$K_{Ic} = 0.59\left(\frac{E}{H}\right)^{\frac{1}{8}}\left(\sigma \cdot P^{\frac{1}{3}}\right)^{\frac{3}{4}} \tag{8}$$

where the true failure stress (σ) was obtained with the use of the stress-strain curves. Five poled-depoled specimens were tested per temperature (Table I). A total of four unpoled specimens was tested at room temperature (Table I). Unlike the true failure stress results, indentation-strength fracture toughness measurements indicate PSZT is relatively temperature insensitive with values ranging between ~1.7 to 2.0 $MPa \cdot m^{1/2}$ (Table I and Fig. 10) from room temperature to 120°C. This is disconcerting because the strength and toughness values should follow the same temperature dependent trend. As a result, the fracture toughness results should be used only as a reference and not as an engineering standard. Several factors could be responsible for this anomaly. For instance, PSZT most likely exhibits R-curve behavior, i.e., toughness increases with crack length. Because toughness measurements were made in the small-crack regime and the indentation-strength technique does not require direct crack measurements, any variations in crack size (for example, due to microstructural heterogeneities) will result in a different calculated toughness value. In addition, the shape of the R-curve may change with temperature because of increased non-linearity; therefore, complicating the toughness-strength relationship. Thus, for R-curve materials, fracture toughness measurements should be performed using techniques where the critical crack size is measured and incorporated into the stress-intensity calculations, such as the surface-crack in flexure technique. For materials that exhibit R-curve behavior, it should be noted that the small-crack regime is of most interest because this will be the most likely failure scenario. In addition to the probable R-curve behavior of PSZT, the fracture toughness results should be considered an approximation because both the indentation-crack length and indentation-strength techniques are susceptible to large systematic errors due to the assumed average geometric and residual stress factors incorporated in Eqs. 6 & 8. These errors may be exacerbated for materials that exhibit non-linear stress-strain behavior.

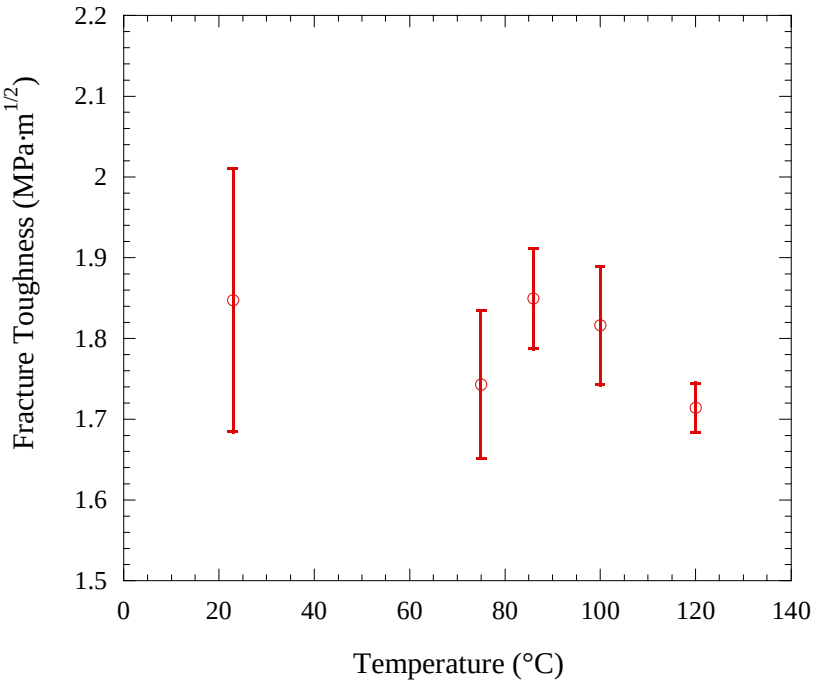

Fig. 10 Average fracture toughness with 95% confidence intervals as determined from the indentation-strength technique from room temperature to 120°C.

Weibull Statistics

Ceramic components are susceptible to failure at stresses much lower than predicted from theoretical calculations because of stress concentration sites at surface or volume flaws, where the location and size of these strength-limiting flaws are randomly distributed. Flaw distributions are processing and handling history dependent, and can vary significantly for ceramic components processed from the same source. Weibull statistics, which are based on weakest link theory, can be employed to estimate the probability of failure for a particular material at a given stress level. An indirect measurement of component reliability can be obtained from the Weibull modulus: a descriptor relating the strength distribution (thus failure-initiating flaw distribution) within the material. A low Weibull modulus is indicative of a material that exhibits a wide range of failure strengths, and thus has a higher probability of failure at a lower stress level than a material exhibiting a higher Weibull modulus. Knowledge of PSZT Weibull parameters is needed to have a more intimate understanding of the effect processing and fabrication conditions have on flaw distributions and ultimately component reliability. As such, Weibull parameters of unpoled and poled-depoled PSZT were determined.

A total of 44 specimens was tested, per processing condition (unpoled or poled-depoled), to failure in 4-point bending. The true failure stress was determined based on the stress-strain results of unpoled and poled-depoled specimens. The strength distribution was characterized using a two-parameter Weibull distribution and maximum likelihood estimators for Weibull modulus (m) and characteristic strength (σ_0)

$$P_f = 1 - \exp\left[-\left(\frac{\sigma}{\sigma_0} \right)^m \right] \tag{9}$$

where P_f is the probability of fracture (Fig. 11). The Weibull modulus for the specimens tested in the unpoled condition was 17 with a characteristic strength of 90.9 MPa and an average strength of 89.4 $\pm$ 1.7 MPa. The strengths ranged from 76 to 99.8 MPa. The poled-depoled specimens exhibited a Weibull modulus of 13.2, a characteristic strength of 92.1 MPa and an average strength of 89.6 $\pm$ 2.6 MPa where the strength values ranged from 68.4 to 102.7 MPa. The lower Weibull modulus indicates that poled-depoled PSZT has a wider flaw distribution compared to unpoled specimens, thus, the pole-depole process could potentially reduce component reliability. The difference in Weibull moduli may be attributed to the additional handling required for the pole-depole step. This includes (i) the application of temporary silver electrodes to the top and bottom surface of the bend bars, (ii) drying of these electrodes at 71°C, (iii) polarization and depolarization in dielectric fluid, (iv) removal of the temporary electrodes with acetone and (v) transportation of specimens between each step. Also, the polarization and then depolarization step could potentially degrade the mechanical properties[16-18] of some specimens as a result of the high electric fields (32 kV/cm) required for this procedure, by creating new flaws or by activating failure initiating flaws at defects that otherwise would have been dormant. However, with the use of fractography it was determined that the lowest strength specimens, unpoled or poled-depoled, typically failed from similar flaws

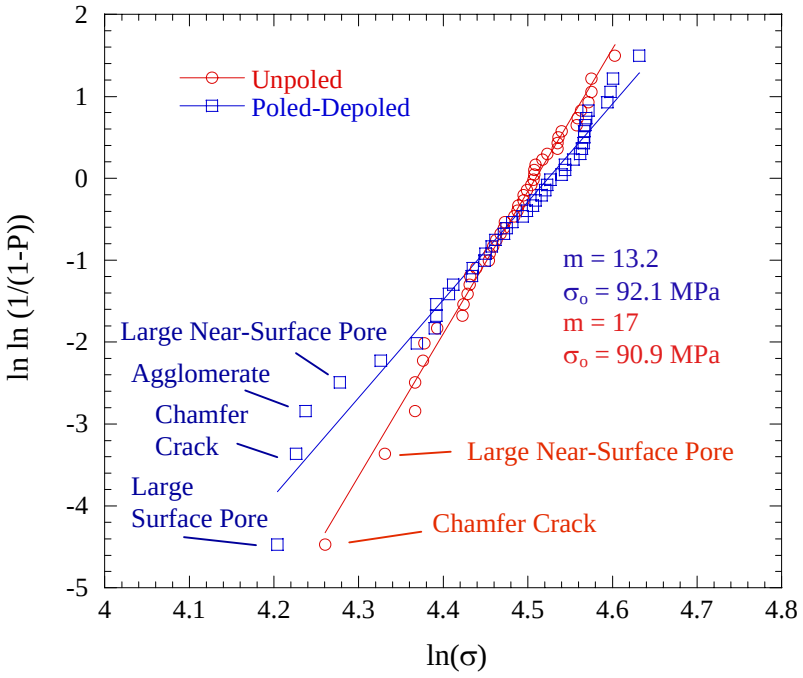

Fig. 11 Weibull plots of strength of unpoled and poled-depoled PSZT. Measurements were made at room temperature on 44 specimens per processing condition.

(Fig. 11). Most likely, a higher number of these gross flaws happened to be sampled for the poled-depoled specimens. By removing the four lowest strength samples from the poled-depoled data set, the Weibull modulus of the poled-depoled specimens was essentially the same as the unpoled Weibull modulus. This suggests that sampling can have a significant effect on the measured Weibull moduli and care should be taken when interpreting the results. From this analysis, the poled-depoled specimens have a slightly lower Weibull modulus than unpoled PSZT; however, the difference in the Weibull moduli may be attributed to the statistical nature of sampling and not the additional processing steps experienced by poled-depoled PSZT.

Fractography

Fracture surfaces were examined to determine failure origins and the type of flaws that initiated failure at low stress levels for both unpoled and poled-depoled specimens (Fig. 11). Examination of fracture surfaces revealed that the majority of failures originated from a combination of large grain clusters and probable machining damage (Fig. 12), surface or near-surface pores and probable machining damage (Fig. 13) or large grain clusters and surface or near-surface pores (Fig. 14). The weakest specimens, however, failed from very large surface or near-surface pores (Fig. 15), agglomerates (Fig. 16) or from large pre-existing cracks located near chamfers.

The reliability of ceramic materials is highly dependent on the presence of handling or machining damage and/or processing flaws. Several of the low strength specimens failed

from pre-existing cracks at the chamfer that may have formed as the result of contact or machining damage. Care must be taken to ensure that the handling and machining of PSZT specimens is innocuous, thus reducing the probability of a large pre-existing crack inducing failure; thereby, increasing the reliability of the component. The reliability of ceramic materials, however, will always be subject to processing and fabrication history as well as handling damage. For instance, the microstructure of ceramics, which is processing history dependent, can be the strength-limiting factor. Microstructural subtleties, such as, abnormally large grains, porosity, agglomerates and/or the presence of second phases can have a significant influence on failure probabilities. Both Figs. 15 & 16 show microstructural features (failure origins) representative of low strength samples. Closer examination of Fig. 15 reveals that, besides the large pore, there is a difference in grain size around the pore compared to that found in the bulk of the material (Fig. 17). This microstructural feature can certainly be a contributor to the low failure stress. In addition, the failure-initiating flaw shown in Fig. 16 appears to be a large agglomerate. At higher magnification, there is noticeable separation between the agglomerate and the bulk (Fig. 18). The cracks associated with the agglomerate led to a very low failure stress (69.2 MPa). Both of these flaws are processing dependent and can be eliminated by modifying processing parameters. Thus, with the use of Weibull statistics the flaw size distribution can be determined and in combination with fractography, failure-initiating flaws can be identified and processing modifications can be implemented to reduce or eliminate these severe flaws. In addition, the reliability of PSZT components can be estimated using computer programs, such as CARES/LIFE[19] or FAILPROB[20], which incorporate Weibull strength statistics into the predicted stress distribution of the component.

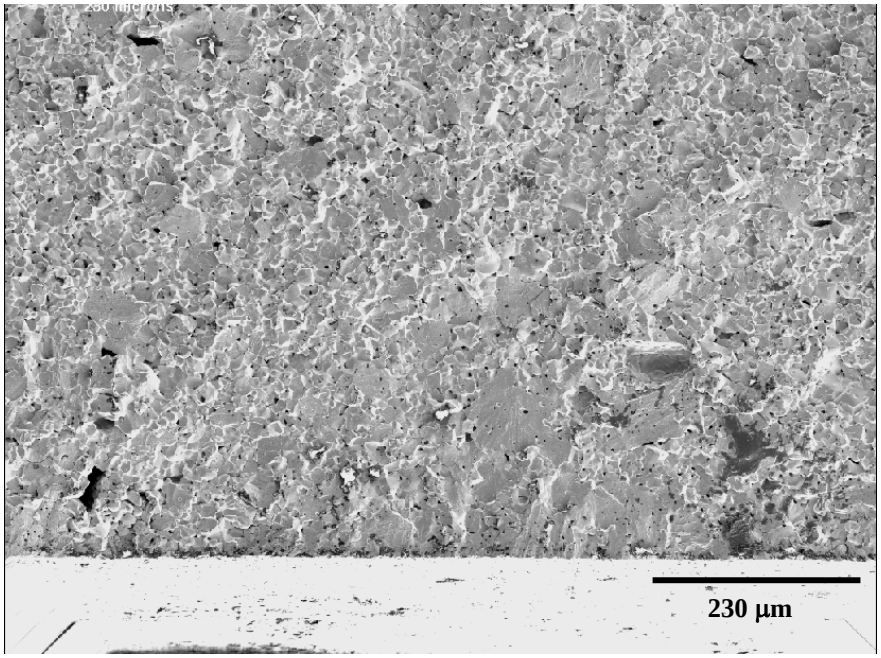

Fig. 12 SEM image showing clusters of large grains in combination with possible machining damage as the failure origin. This specimen exhibited a failure stress of 91.5 MPa.

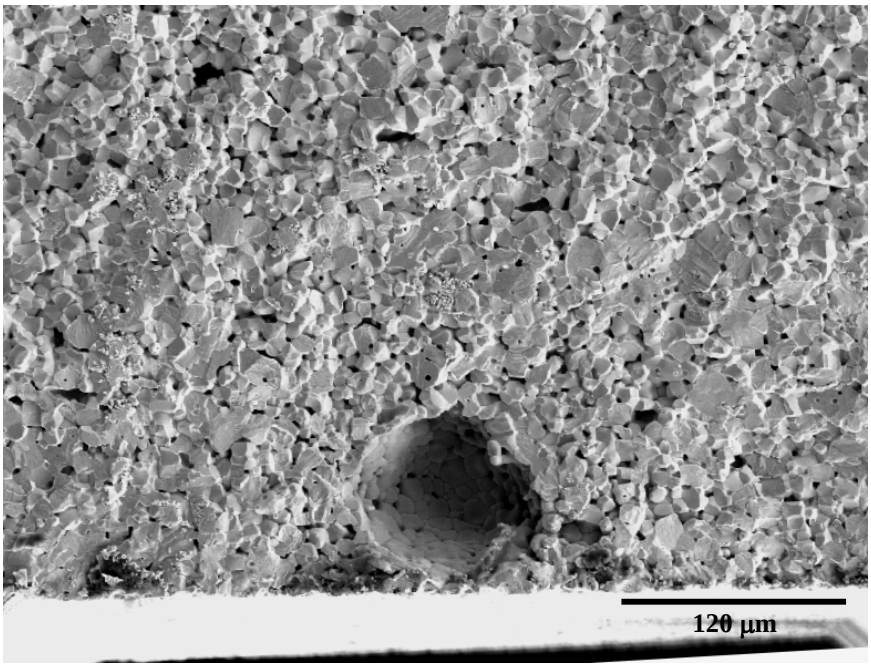

Fig. 13 SEM image showing a representative fracture surface of a near-surface pore in combination with possible machining damage. This specimen failed at 86.1 MPa.

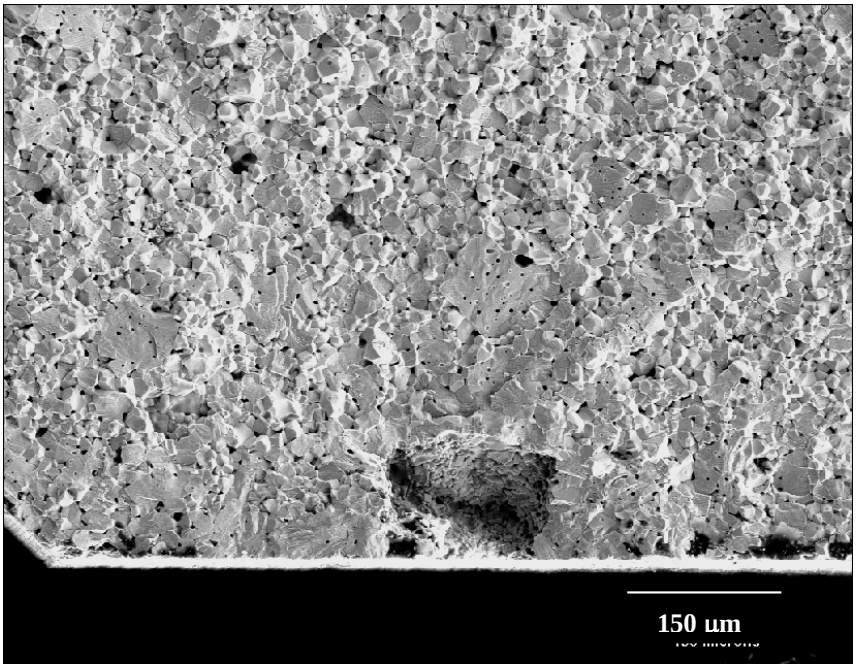

Fig. 14 SEM image of a fracture surface with a failure origin consisting of a combination of large grains and a surface pore. This specimen failed at 92.5 MPa.

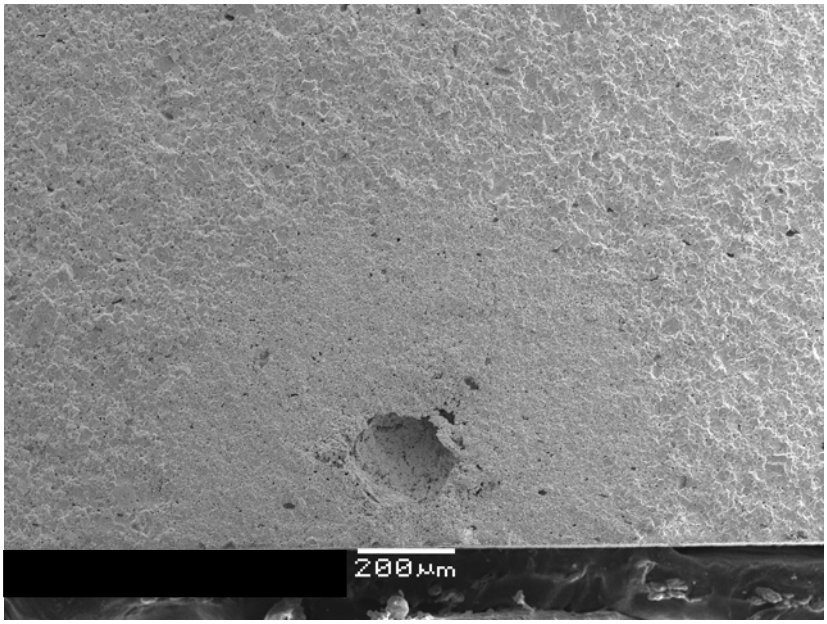

Fig. 15 SEM image of a fracture surface where a large near-surface pore initiated failure at a stress of 72.1 MPa.

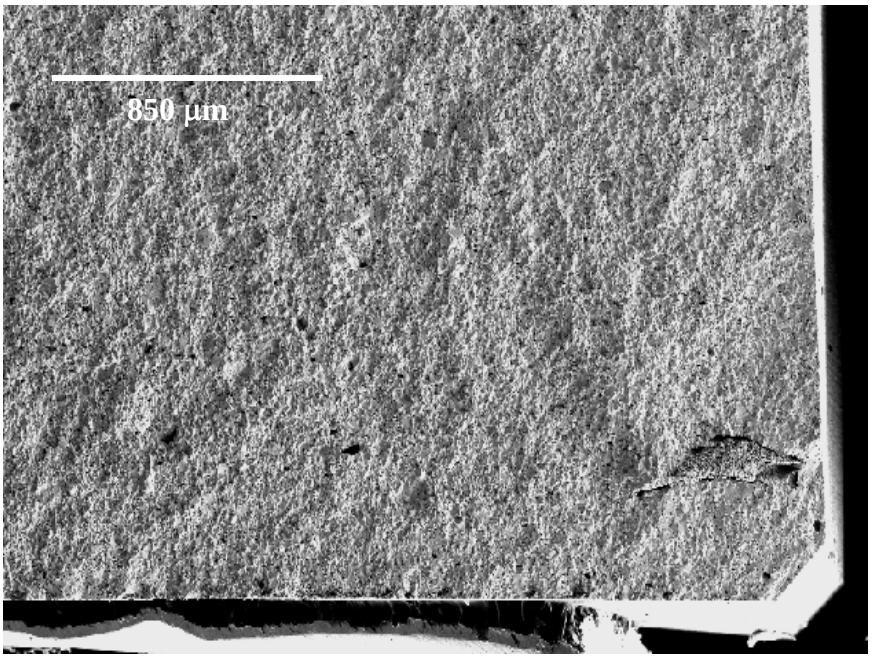

Fig. 16 SEM image of what appears to be an agglomerate where failure initiated. This specimen failed at a stress of 69.2 MPa.

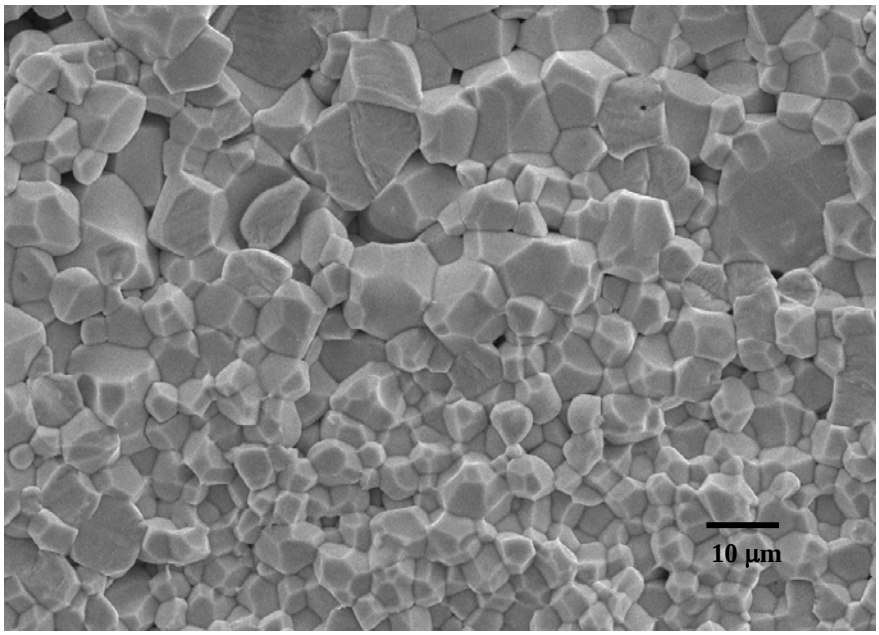

Fig. 17 SEM image of a fracture surface showing a distinct boundary between small and large grains. The small grains surround a large pore.

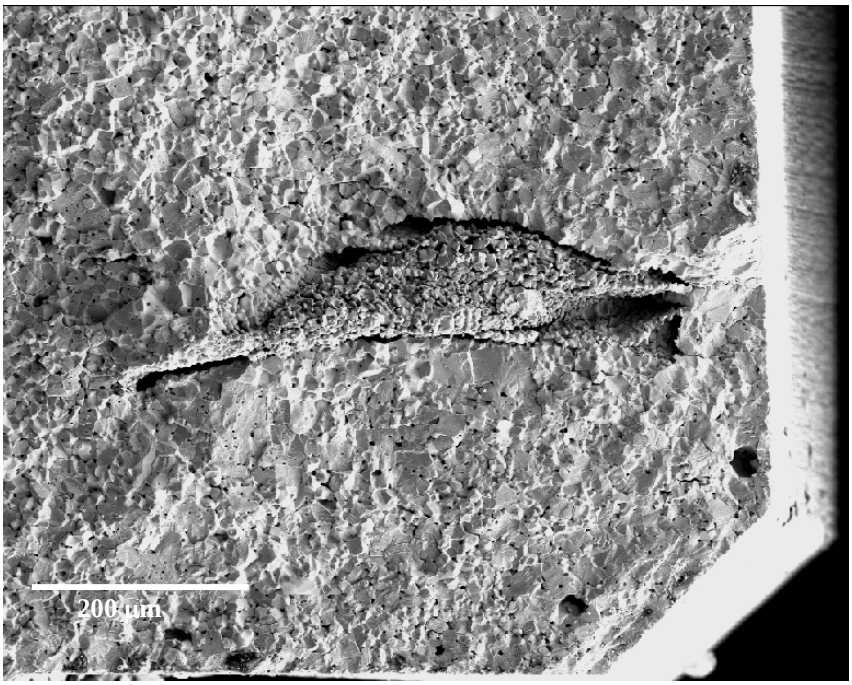

Fig. 18 SEM image of a processing flaw (large agglomerate) that was responsible for failure.

SUMMARY

Strength, fracture toughness and the stress-strain behavior of PSZT were determined as a function of temperature (23, 75, 86, 100 and 120°C). The strength of PSZT decreases with temperature. Strength measurements were carried out with the use of strain gauges and an extensometer in order to evaluate the true stress-strain behavior. PSZT undergoes non-linear and non-symmetric stress-strain behavior, which is more predominate at elevated temperatures. A comparison of the strain gauge and extensometer techniques indicates only a slight difference (~3%) in the calculated true failure stress. Both measurement techniques indicate a significant reduction in the outer-fiber stress at failure as temperature increases. The implications of this are that if the assumption of linear-elasticity was used a systematic overestimation in the failure stress would result. The load-carrying capacity of PSZT does not change as a function of temperature, but the extent of deformation does increase with temperature. Unlike the true failure stress results, indentation-strength measurements indicate that the fracture toughness of PSZT is temperature independent. These results are contrary to the typical toughness-strength relationship exhibited by brittle materials; this difference may be the result of R-curve behavior and/or non-linearity. Additional tests using direct crack length measurements, such as the surface-crack in flexure technique, are needed to determine the true fracture toughness of PSZT as a function of temperature. The Weibull parameters of PSZT indicate that poled-depoled specimens have a slightly higher probability of failure at a particular stress level (thus lower reliability) than unpoled PSZT. Thorough examinations of the fracture surfaces, however, suggest that the lower Weibull modulus of poled-depoled PSZT may be attributed to sampling rather than differences resulting from additional processing.

REFERENCES

1. R.H. Moore, G.R. Burns, S.N. Burchett, S.J. Glass, M.A. Hutchinson, T.W. Scofield, M.E. Stavig, C.S. Watson, and P. Yang, "Polarization Induced Cracking in Partially Electroded PSZT Ceramic," *Sandia National Laboratories Report*, SAND2002-2384C (2002).
2. S.L.d.S.e. Lucato, D.C. Lupascu, and J. Rodel, "Crack Initiation and Crack Propagation in Partially Electroded PZT," *Journal of the European Ceramic Society*, **21** 1425-1428 (2001).
3. S. Lucato, D. Lupascu, M. Kamlah, J. Rodel, and C. Lynch, "Constraint-Induced Crack Initiation at Electrode Edges in Piezoelectric Ceramics," *Acta Materialia*, **49** [14] 2751-2759 (2001).
4. A. Furuta and K. Uchino, "Dynamic Observation of Crack-Propagation in Piezoelectric Multilayer Actuators," *Journal of the American Ceramic Society*, **76** [6] 1615-1617 (1993).
5. R.F. Cook, S.W. Freiman, and B.R. Lawn, "Fracture of Ferroelectric Ceramics," *Ferroelectrics*, **50** 267-272 (1983).

6. R. Fu and T.Y. Zhang, "Influences of Temperature and Electric Field on the Bending Strength of Lead Zirconate Titanate Ceramics," *Acta Materialia*, **48** [8] 1729-1740 (2000).
7. K. Mehta and A.V. Virkar, "Fracture Mechanisms in Ferroelectric-Ferroelastic Lead Zirconate Titanate [Zr-Ti=0.54-0.46] Ceramics," *Journal of the American Ceramic Society*, **73** [3] 567-574 (1990).
8. "Standard Test Method for Flexural Strength of Advanced Ceramics at Ambient Temperatures," *ASTM Designation C1161-02c*, American Society for Testing and Standards, West Conshohocken, Pennsylvania.
9. G. Anstis, P. Chantikul, B. Lawn, and D. Marshall, "A Critical-Evaluation of Indentation Techniques for Measuring Fracture-Toughness .1. Direct Crack Measurements," *Journal of the American Ceramic Society*, **64** [9] 533-538 (1981).
10. P. Chantikul, G. Anstis, B. Lawn, and D. Marshall, "A Critical-Evaluation of Indentation Techniques for Measuring Fracture-Toughness .2. Strength Method," *Journal of the American Ceramic Society*, **64** [9] 539-543 (1981).
11. A. Nadai, *Theory of Flow and Fracture of Solids*, 2nd ed. McGraw-Hill, New York, 1950, Vol. 1, p. (Chapter 22).
12. W. Chen, D. Lupascu, J. Rodel, and C. Lynch, "Short Crack R-curves in Ferroelectric and Electrostrictive PLZT," *Journal of the American Ceramic Society*, **84** [3] 593-597 (2001).
13. T. Fett, S. Muller, D. Munz, and G. Thun, "Nonsymmetry in the Deformation Behaviour of PZT," *Journal of Materials Science Letters*, **17** [4] 261-265 (1998).
14. G.A. Gogotsi, "The Problem of the Classification of Low-Deformation Materials Based on the Features of Their Behavior Under Load," *Strength of Materials*, **9** [1] 77-83 (1977).
15. J.H. Gieske, "Elastic Property Measurements of PSZT HF6104 versus Temperature from 22 to 130°C," internal memorandum to P. Yang, Sandia National Laboratories, Albuquerque, New Mexico, January 29, 2002.
16. A.G. Tobin and Y.E. Pak, "Effect of Electric Fields on Fracture Behavior of PZT Ceramics," *Proceedings of the SPIE The International Society for Optical Engineering*, **1916** 78-86 (1993).
17. K.D. McHenry and B.G. Koepke, "Electric Field Effects on Subcritical Crack Growth in PZT," *Fracture Mechanics of Ceramics*, **5** 337-352 (1983).
18. S. Park and C. Sun, "Fracture Criteria for Piezoelectric Ceramics," *Journal of the American Ceramic Society*, **78** [6] 1475-1480 (1995).
19. N.N. Nemeth, L.M. Powers, L.A. Janosik, and J.P. Gyekenyesi, "CARES/Life Ceramics Analysis and Reliability Evaluation of Structures," *Users and Programmers Manual*, NASA TM-106316.
20. G.W. Wellman, "FAILPROB--A Computer Program to Compute the Probability of Failure of a Brittle Component," *Sandia National Laboratories Report*, SAND2002-0409 (2002).

APPENDIX

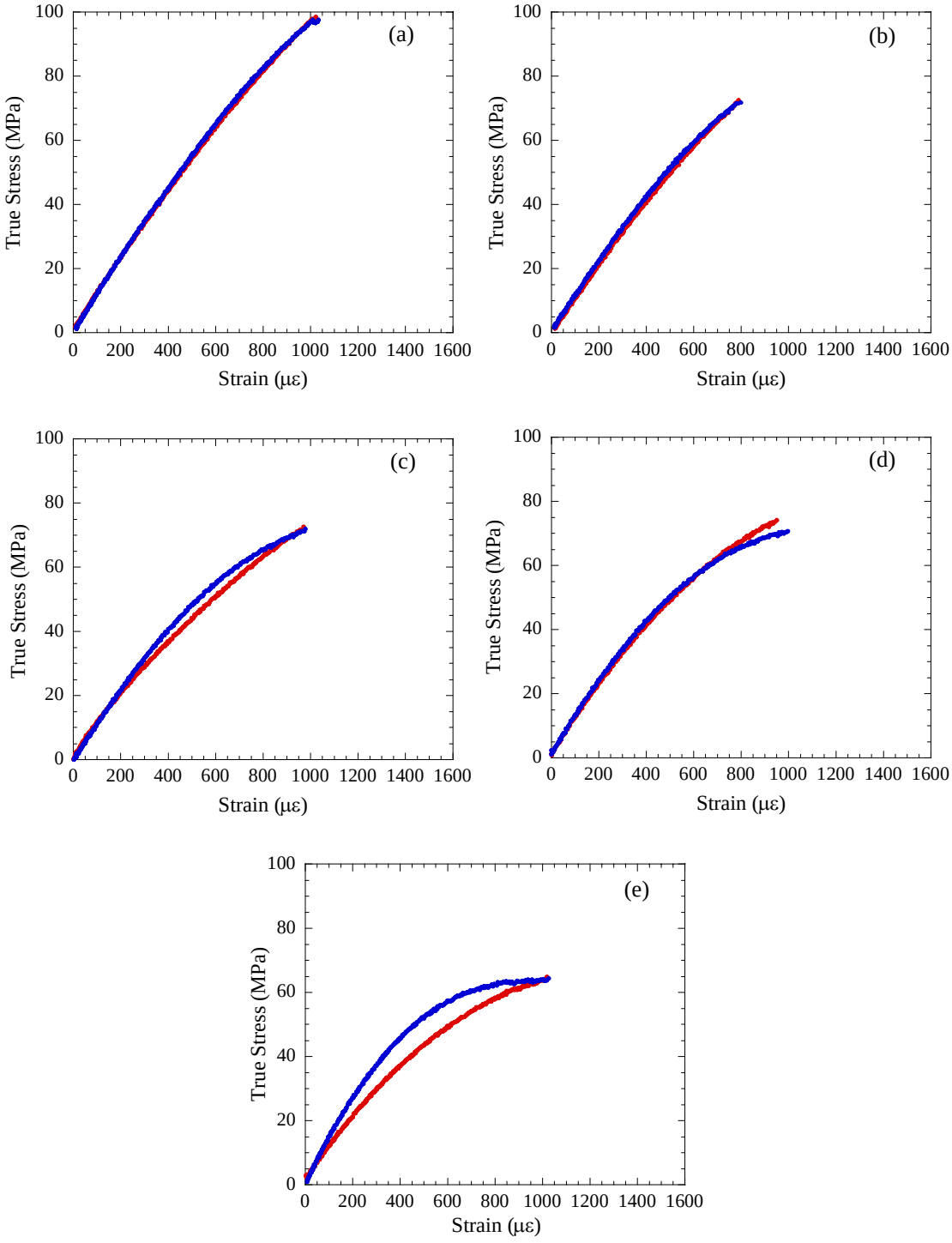

Fig. I Some tests did not show the significant differences between the tension (blue) and compression stress-strain (red) curves that is demonstrated in Fig. 8. This could be due to factors including strain-gauge misalignment, poor strain-gauge adhesion, or statistical variations in mechanical data. Measurements were made at (a) 23, (b) 75, (c) 86, (d) 100 and (e) 120°C.

DISTRIBUTION:

1	MS 0415	D.H. Zeuch, 09741
1	0515	J.D. Keck, 02561
1	0521	S.T. Montgomery, 02561
1	0521	T.W. Scofield, 02561
1	0553	J.R. Laing, 09123
1	0819	J. Robbins, 09231
1	0847	S.N. Burchett, 09126
1	0869	N.A. Lapetina, 14402
1	0885	D.B. Dimos, 01801
1	0886	B.B. McKenzie, 01822
1	0889	S.J. Glass, 01843
1	0889	S.L. Monroe, 01843
1	0889	C. Newton, 01843
1	0889	R. Tandon, 01843
5	0889	C.S. Watson, 01843
1	0961	C. Adkins, 14100
1	0959	G.R. Burns, 14192
1	0959	T.J. Gardner, 14192
1	0959	M.A. Hutchinson, 14192
1	0959	R.H. Moore, 14192
1	0959	P. Yang, 14192
1	1349	W.F. Hammetter, 01843
1	1411	M.V. Braginsky, 01843
1	1411	V. Tikare, 01834
1	1411	B.A. Tuttle, 01843
1	MS9018	Central Technical Files, 8945-1
2	0899	Technical Library, 9616
1	0612	Review & Approval Desk, 9612 For DOE/OSTI